Observation of topological surface states in the high-temperature superconductor MgB,

Huaqing Huang,² Gang Cao,¹ Nikolai D. Zhigadlo⁰,^{3,4} Feng Liu,^{2,5} and Daniel S. Dessau^{1,6,†} ¹Department of Physics, University of Colorado at Boulder, Boulder, Colorado 80309, USA ²Department of Physics, University of Utah, Salt Lake City, Utah 84112, USA ³Department of Chemistry and Biochemistry, University of Bern, CH-3012 Bern, Switzerland ⁴CrystMat Company, CH-8046 Zurich, Switzerland ⁵Collaborative Innovation Center of Quantum Matter, Beijing, 100084, China ⁶Center for Experiments on Quantum Materials, University of Colorado at Boulder, Boulder, Colorado 80309, USA

(Received 20 November 2018; revised manuscript received 22 October 2019; published 21 November 2019)

Most topological superconductors known to date suffer from low transition temperatures (T_c) and/or high fragility to disorder and dopant levels, which is hampering the progress in this promising field. Here, utilizing a combination of angle-resolved photoemission spectroscopy measurements and density-functional theory calculations, we show the presence of a type of topological Dirac nodal line surface state on the [010] faces of the $T_c = 39$ K BCS superconductor MgB₂. This surface state should be highly tolerant against disorder and inadvertent doping variations and is expected to go superconducting via the proximity effect to the bulk superconductor that this state is intimately connected to. This would represent a form of high-temperature topological superconductivity.

DOI: 10.1103/PhysRevB.100.184511

I. INTRODUCTION

As its name suggests, a topological superconductor needs two essential ingredients: nontrivial topology and the superconducting order. Initially, the exploration of topological superconductivity was limited to the 5/2 quantum Hall state in electron gas systems [1-3] and p-wave superconductors such as Sr₂RuO₄ [4–6], in which the chiral superconducting order parameter is topologically nontrivial by itself. However, these systems are extremely sensitive to disorder, very scarce in nature, and have transition temperatures well below liquid helium temperature—each of which imposes great difficulties in the exploration of topological superconductivity. The discovery of topological band structures [7,8] introduces an alternative and arguably more favorable recipe—that the "topological" part of a topological superconductor can be substituted by a topological surface state (TSS). In systems with both topologically nontrivial band inversions and conventional s-wave superconducting gaps [9], the topological surface state can be gapped by the superconducting gap [10–12] through the proximity effect and enables topological superconductivity. To avoid the complications of interface physics, it is preferable to use a single system, such as the one discussed here.

To make a singular topological superconductor, researchers have devoted a great deal of effort into doping known bulk topological material, which has seen some success in materials such as Cu-doped Bi₂Se₃ [13-15]. However, given that the discoveries of high-temperature superconductivity have been largely accidental, it is unclear how far this approach can go. Here we adopt an alternative approach by looking for topological surface states in known high-temperature superconductors—and MgB₂ ranks high on this list. At ambient pressure, its superconducting transition temperature of 39 K [16] is the highest among conventional s-wave superconductors, and second only to certain members of the cuprate and pnictide family among all known superconductors. Very recently, a particularly promising candidate $FeTe_{1-x}Se_x$ [17] was found in the family of pnictide high-temperature superconductors, with a transition temperature of 14.5 K setting the current record. While this discovery is exciting, the required proximity of a very small (20-meV scale) spin-orbit-coupled gap to the Fermi energy means that the system should be highly sensitive to inadvertent doping variations.

Although MgB₂ as a high-temperature superconductor has been extensively studied by many techniques including angleresolved-photoemission spectroscopy (ARPES) [18-22], its ability to harbor topological surface states has never been appreciated. In this work, we use a combination of firstprinciple density-functional theory (DFT) calculations and ARPES to look for topological surface states in MgB2. Our DFT calculations [23] have predicted the existence of pairs of topological Dirac nodal lines [24] at the Brillouin-zone boundaries, as well as topological surface bands that connect these nodal lines. The calculations further predict that the topological surface states should be robust against realistic doping variations, and readily gapped by the superconducting order, as expected by the intimate and inherent contact between the bulk superconducting states and the topological surface states.

^{*}Xiaoqing.Zhou@Colorado.edu

[†]Dessau@Colorado.edu

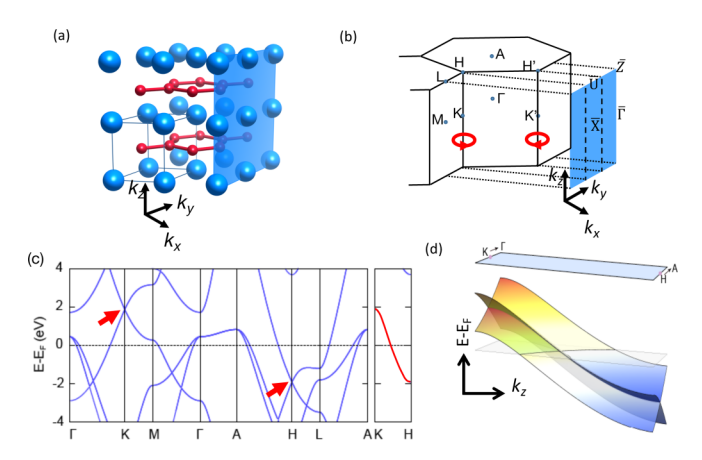


FIG. 1. (a) Crystal structure of MgB₂ with hexagonal lattice in the ab plane, determined by x-ray diffraction. The face of the edge cleave is shown in blue, and the cleaved surface can be either Mg- or B terminated. (b) The 3D Brillouin zone and the projected "zigzag" [010] surface Brillouin zone (shown as the blue sheet). High-symmetry points K/H and K'/H' come in mirror-symmetric pairs, with Berry phase of π and $-\pi$, respectively. (c) Calculated DFT bulk band structure along the high-symmetry cut showing Dirac points (red arrows) along K-H. (d) Illustration of a Dirac nodal line along K-H, with Dirac point exactly meeting E_F midway along the cut. The k_x direction is normal to the [010] surface and so is covered by varying photon energy, in our case from 30 to 140 eV.

II. RESULTS

The key to the topological surfaces states are the topological Dirac nodal lines, with associated Dirac points on high-symmetry cuts [highlighted by the arrows in the band-structure plot of Fig. 1(c)]. As illustrated by Fig. 1(d), the Dirac nodal line disperses across $E_{\rm F}$ in the k_z direction

(normal to the honeycomb layers) over a few eV range, so that Dirac band crossings as well as the corresponding topological surface states will always be present at $E_{\rm F}$ for essentially any conceivable amount of doping or band-bending effects. As shown in Fig. 1(b), the Dirac nodal lines predicted by the DFT calculation are located at the zone boundary of the 3D Brillouin zone along the K-H and K'-H' high-symmetry lines that run along the z axis. Our calculations (see Supplemental Material [25] and references [1,2] therein) show that each of these nodal lines in MgB $_2$ is wrapped by a Berry phase of π , i.e., they support a Z_2 topology. Similar to the case in graphene, the K'-H' line can be regarded as the mirror image of the K-H, so the associated Berry phase for the K'-H' nodal line is $-\pi$ instead of π for the K-H nodal line.

Because of their k_z dispersion, the Dirac nodal lines can be best accessed from the side so that the dispersion is in the experimental plane a geometry different from all previous ARPES experiments that studied the sample from the c axis, which is also the natural cleavage face. For our experiment we cleaved the samples from the "side" [blue plane of Figs. 1(a) and 1(b)] and performed ARPES on that thin [010] face—a challenging but achievable task. The cleaved surface viewed with a scanning electron microscope [see Fig. 2(b)] as well as an atomic force microscope (see Supplemental Material [25] and references [3–8] therein) shows an atomically flat region, upon which high-quality ARPES spectra were observed at 10 K. We measured the band dispersion along the momentum perpendicular to the cleavage face (k_x) by scanning the photon energy hv from 30 to 138 eV along the Γ -K high-symmetry line with linear s polarization. Since at these photon energies the photon momentum is negligible, we have [26]

$$k_x \approx \sqrt{\frac{2m_e}{\hbar^2}(h\nu - \emptyset - E_B + V_0) - (k_y^2 + k_z^2)},$$
 (1)

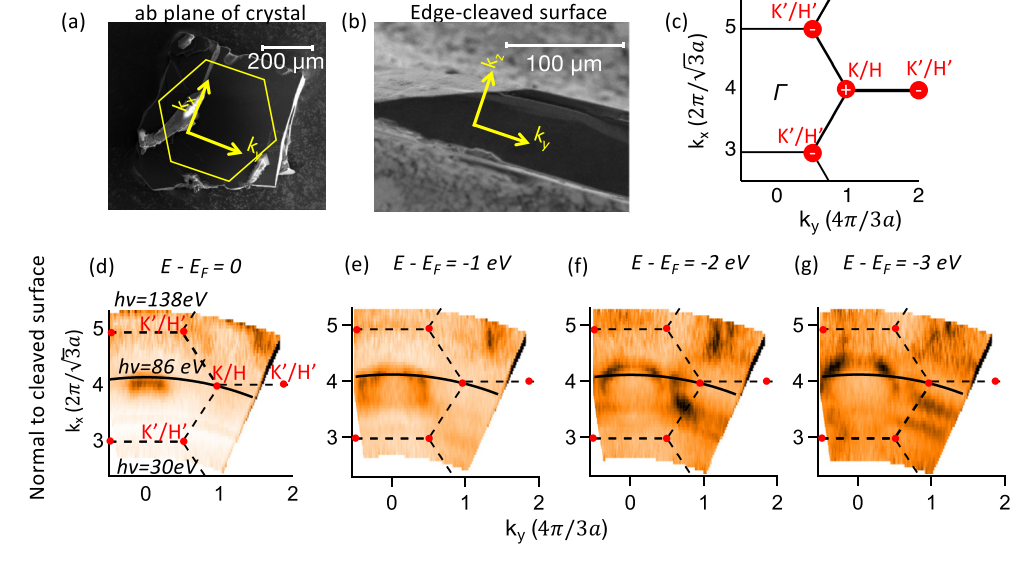


FIG. 2. Edge-on ARPES gives in-plane bulk electronic structure. (a), (b) In-plane and edge-cleaved views of our crystals, respectively. Crystal orientation is obtained through x-ray diffraction. (c) In-plane Brillouin-zone points. (d)–(g) In-plane isoenergy ARPES plots at energies from E_F to -3 eV. The k_y direction is parallel to the cleaved surface (panel b) and so is covered by varying the emission angle. The k_x direction is normal to the edge-cleaved surface and is covered by varying the incident photon energy from 30 eV (low k_x) to 138 eV (higher k_x). The solid line representing 86 eV cuts through the K/H Brillouin zone point.

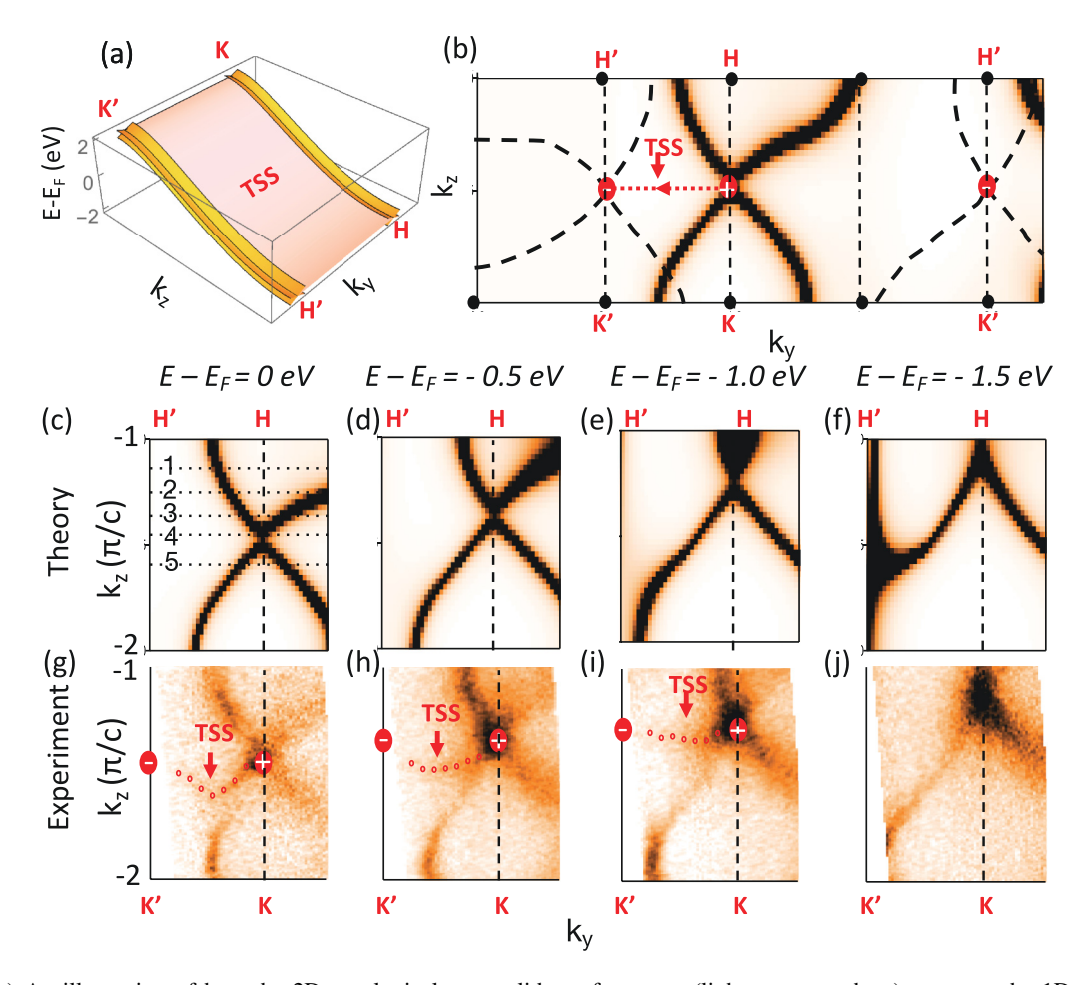


FIG. 3. (a) An illustration of how the 2D topological water-slide surface state (light magenta sheet) connects the 1D nodal lines. (b) Illustration of the K/H and K'/H' Dirac nodal lines with the Z_2 Berry-phase monopoles (+ and -) projected to the 2D cleaved surface. The plot is made for the photon energy 86 eV [$k_x \approx 4$ in the units of Fig. 2(c)] that due to the proper k_x value can access the bulk Fermi surface in the center of the plot. The dashed bulk Fermi surface shown at the left and right are at incorrect k_x values to be observed. A topological surface state connecting the +1 and -1 monopoles on the projected surface Brillouin zone is drawn in by hand. (c)-(f) DFT spectral function convoluted by a Gaussian function (to simulate band broadening) in the $k_y - k_z$ plane at 86 eV at a variety of binding energies. (g)-(j) Experimentally measured isoenergy contours using 86-eV photons. In addition to the excellent agreement between the predicted and measured bulk states, we identified an additional set of surface states (open circles) through Lorentzian fitting of momentum distribution curves along k_z (see Supplemental Material [25], Fig. S3). This surface state connects the pairs of Dirac points as predicted; therefore it is labeled as TSS (Topological Surface State or surface Fermi arc). The weak spectral intensity of the surface states is expected for a surface with cleavage imperfections or disorder.

where $\emptyset = 4.3$ eV is the work function, E_B the binding energy, and $V_0 = 17 \text{ eV}$ the inner potential. This describes the ARPES spectra measured on a "spherical sheet," the radius of which is proportional to $\sqrt{h\nu - \emptyset - E_B + V_0}$. By stitching together many spectra taken over a wide range of photon energies from 30 to 138 eV, we reconstruct the isoenergy plots in the [001] plane at $k_z = 0$, as shown in Figs. 2(d) to 2(g). The data show a spectra consistent with previous ARPES studies on the [001] cleavage plane [18-22] (see Supplemental Material [25]). This confirms that we are able to observe the proper bulk band structure of MgB₂ from the cleaved [010] plane. As illustrated in Fig. 2(c), in our experimental geometry the K-H Dirac nodal line acts as a monopole of Berry phase and is neighbored by three of its "mirror-image" K'-H' lines with opposite charge, each of which has bulk bands accessible only under different experimental conditions (i.e., photon energies and experimental angles). We choose the photon energy $h\nu =$ 86 eV (black line in the panels), which allows us to directly access one of the K-H high-symmetry lines by varying the k_z momentum axis.

To better investigate the Dirac nodal line, Fig. 3 focuses on the region near the high-symmetry line K-H at $k_x \approx 8\pi/\sqrt{3}a$, $k_y = 4\pi/3a$, and $k_z \sim \pi/c$ to $2\pi/c$. As shown in Fig. 3(a), on the projected surface Brillouin zone we should expect a 2D topological surface state (TSS) connecting a pair of 1D Dirac nodal lines with opposite charges [27], as any loop encircles the nodal lines will pick up a Berry phase of π or $-\pi$. This "water-slide" TSS is analogous to the flat "drumhead" surface state in Dirac nodal loop systems [28], but follows the dispersions of the nodal lines over a range of \sim 4 eV. Viewed from the sample projection [Fig. 3(b)], the topological surface states could connect the $+\pi$ nodal line $(k_y = 4\pi/3a)$ to the $-\pi$ nodal line on the left $(k_y = 2\pi/3a)$, or the one on the right $(k_y = 8\pi/3a)$, but not both. As shown

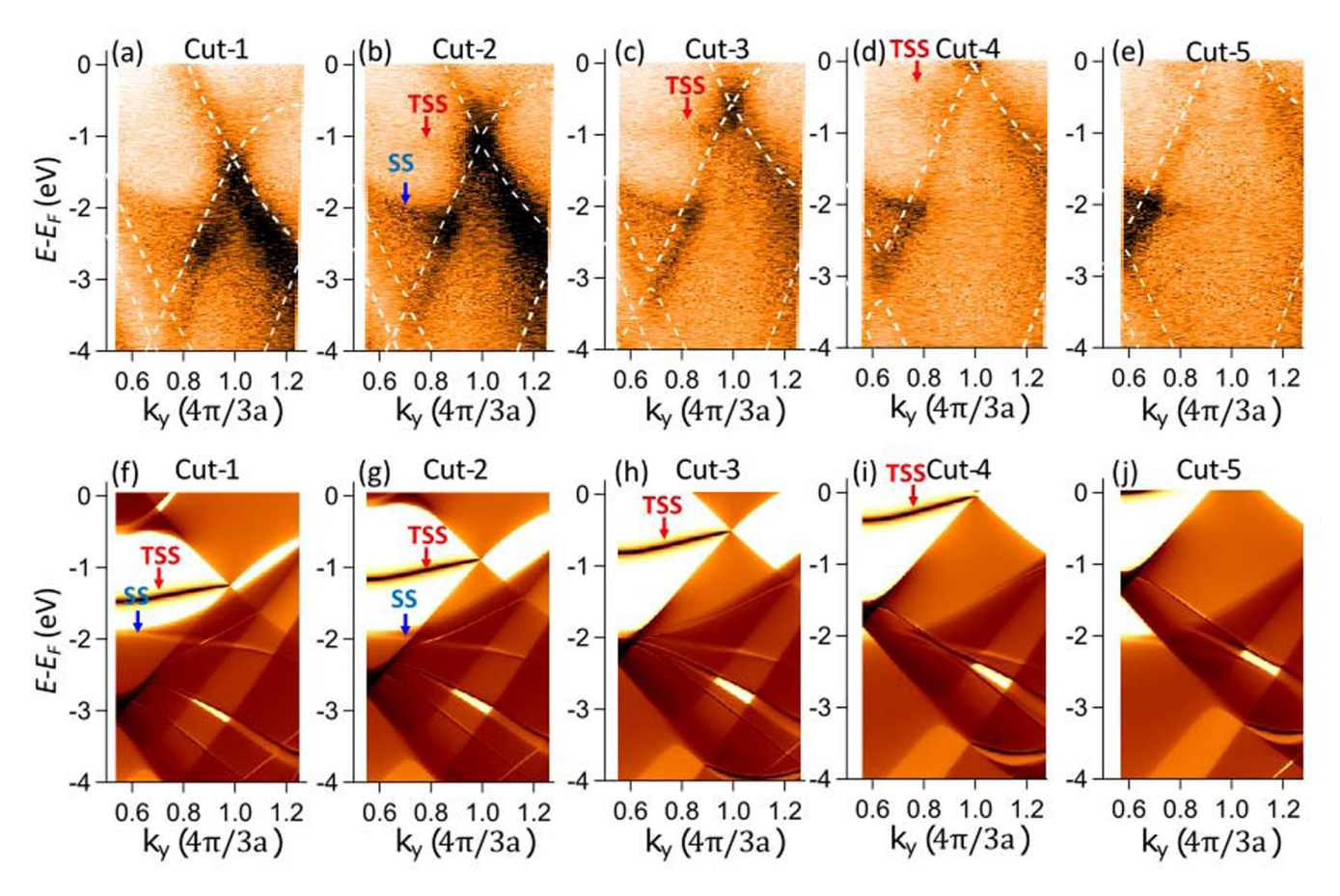


FIG. 4. TSS's emanating from Dirac points. (a)–(e) ARPES spectra from the five cuts of Fig. 3(c), overlapped by DFT calculations (white dashed lines). The Dirac band crossings evolve from below E_F to above E_F consistent with the diagram of Fig. 1(d). Through second derivative analysis (see Supplemental Material [25], Fig. S4), we identified nearly flat topological surface states (red open circles) in cuts (b)–(d), which connect to the Dirac points and similarly move up in energy. In contrast, regular (nontopological) surface states (indicated by the blue arrows) remain relatively "static" in energy in all five cuts. (f)–(j) DFT simulation of spectral intensity, convolved by a Gaussian function to simulate band broadening. The calculated DFT points have been shifted up by 0.5 eV relative to the measured spectra.

in Figs. 3(b) to 3(i), we have excellent agreement between the DFT bulk band calculations and the ARPES isoenergy plots, in which the shifting touching point of an electron pocket and a hole pocket indicates nontrivial band crossings dispersing along K-H. Importantly, through momentum distribution curves analysis (see Supplemental Material [25]) we found an additional feature originating from the touching point that is absent from the DFT calculations of the bulk bands. It looks similar to a "Fermi arc" in Weyl semimetal [29], but persists for most binding energies (E-E_F) and connects towards the $-\pi$ bulk band crossing point at $k_y = 2\pi/3a$, even though the corresponding bulk bands are not experimentally accessible at 86 eV. These look like the TSS's drawn in Fig. 3(b) and we label them as such, though confirmation from an energy cut (Fig. 4) is still required.

To further confirm the topological nature of the surface state, in Fig. 4 we plot the dispersion along five cuts across the touching points [dotted lines in Fig. 3(c)]. As the predicted Dirac nodal line should disperse along the K-H high-symmetry cut, the band crossings should evolve continuously from below E_F to above E_F as shown in Fig. 1(c). This is exactly what we observed, confirming the Dirac nodal line nature of these states. We directly overlay the DFT

calculations of the bulk band dispersions (white dashed lines) with the ARPES spectra with no alteration of the masses or velocities, and a -0.5 eV offset in the DFT chemical potential (possibly due to the depletion of Mg or B atoms on the surface). The agreement is overall excellent, with the chemical potential shift indicative of extra electron charge leaving the cleaved surface. In particular, we stress that over a huge range of possible chemical shifts (such as those induced by unintentional doping), here the Dirac nodal lines dispersing along K-H guarantees Dirac points and topological surface states right at E_F , in sharp contrast to the case of FeTe_{1-x}Se_x (see Supplemental Material [25] for more discussions). In addition to the agreement with the bulk Dirac nodal line, the experiment shows some additional weak features which is captured by second derivative analysis (see Supplemental Material [25]). As all bulk bands are accounted for, these should be of nonbulk origin, i.e., surface states. Most interesting of these are the ones highlighted in red that are observed to connect to the Dirac points in both energy space (Fig. 4) and momentum space (Fig. 3), with this effect observed over a wide range of energies and momenta. Away from the Dirac point its dispersion is much flatter than the bulk band in the s-p metal MgB₂. This is fully consistent with the existence of a topological surface state that we theoretically predicted to connect the Dirac points on this particular surface [23], and we label it as such. This state contrasts with a topologically trivial surface state (blue arrow) that is largely insensitive to the energy of the Dirac point as it disperses from cut to cut.

III. DISCUSSION

These topological surface states are expected to go superconducting via the proximity effect, which would make this material by far the highest transition temperature and most robust topological superconductor, and an excellent platform for a multitude of future studies. Even higher-energy resolution ARPES than what we have carried out here could be utilized to directly detect a superconducting gap in the TSS's, although this is nontrivial since the highest-resolution ARPES facilities are mostly laser ARPES [30,31], which lack the ability to reach the relevant k-space locations. Scanning tunneling microscopy (STM) could also potentially be utilized to detect such a gap. Regardless, since the contact between the topological surface states with the bulk superconductivity is almost guaranteed to be near ideal since the surface states are an intrinsic part of the electronic structure, this next step is highly likely to be realized. On the other hand, further explorations of MgB₂ still face quite a few of their own technical difficulties—that the (010) faces of single crystals are very small and difficult to work with, calling for atomically flat thin films [32] on the [010] face. A different probe, such as STM [33], might provide vital insights into this exploration, too.

The observation of the topological surface state confirms the theoretical prediction of MgB_2 as a promising topological superconductor candidate. Given that there are no topological surface states near the Fermi energy in cuprate superconductors, and that the transition temperature in the best pnictides

superconductors are not much higher, the potential topological superconductivity in MgB_2 would not only set the current record for T_c among topological superconductors but also approach the realistic limit. More important than the high T_c , however, is the fact that the topological surface state that is now expected in this material should be much less sensitive to disorder or dopant variations than in other topological superconductors, including the discovered state in FeSe_{0.45}Te_{0.55} [17]. MgB_2 thus has the best of these two ingredients, i.e., a high superconducting transition temperature and a robust topological surface state.

Last, the success in the conventional superconductor MgB_2 helps guide the hunt of topological superconductors to a different direction: since the topological surface state associated with Dirac nodal lines and loops seems to be more abundant [34] than that of high-temperature superconductivity, we should optimize the weak link, and search for superconductors that have topological band structures or can be made topological.

ACKNOWLEDGMENTS

We thank Drs. D. H. Lu, Dr. M. Hashimoto, and Dr. T. Kim for technical assistance on the ARPES measurements. We thank Dr. R. Nandkishore and Dr. Qihang Liu for useful discussions. The photoemission experiments were performed at beamline 5-2 of the Stanford Synchrotron Radiation Lightsource and the Diamond Light Source beamline I05 (Proposal No. SI17595). This work was funded by DOE Project No. DE-FG02-03ER46066 (Colorado) and by the DOE Project No. DE-FG02-04ER46148 (Utah). The Stanford Synchrotron Radiation Lightsource is supported by the Director, Office of Science, Office of Basic Energy Sciences, of the US Department of Energy under Contract No. DE-AC02-05CH11231. Work at Cao's lab was supported by NSF via grants DMR 1712101 and DMR 1903888.

G. Moore and N. Read, Non-abelians in fractional quantum Hall effect, Nucl. Phys. B 360, 362 (1981).

^[2] B. I. Halperin and A. Stern, Proposed Experiments to Probe the Non-Abelian v = 5/2 Quantum Hall State, Phys. Rev. Lett. **96**, 016802 (2006).

^[3] P. Bonderson, A. Kitaev, and K. Shtengel, Detect Non-Abelian Statistics in the $\nu=5/2$ Fractional Quantum Hall State, Phys. Rev. Lett. **96**, 016803 (2006).

^[4] S. Das Sarma, C. Nayak, and S. Tewari, Proposal to stabilize and detect half-quantum vortices in strontium ruthenates thin films: Non-Abelian braiding statistics of vortices in a $p_x + ip_y$ superconductor, Phys. Rev. B **73**, 220502(R) (2006).

^[5] C. Kallin, Chiral p-wave order in Sr₂RuO₄, Rep. Prog. Phys. 75, 042501 (2012).

^[6] Y Maeno, S. Kittaka, T. Nomura, S. Yonezawa, and K. Ishida, Evaluation of spin-triplet superconductivity in Sr₂RuO₄, J. Phys. Soc. Jpn 81, 011009 (2012).

^[7] L. Fu, C. L. Kane, and E. J Mele, Topological Insulators in Three Dimensions, Phys. Rev. Lett. **98**, 106803 (2007).

^[8] C. L. Kane and M. Z. Hasan, Topological insulators, Rev. Mod. Phys. 82, 3045 (2010).

^[9] L. Fu and C. L Kane, Superconducting Proximity Effect and Majorana Fermions at the Surface of a Topological Insulator, Phys. Rev. Lett. 100, 096407 (2008).

^[10] L. S. Wray, S.-Y. Xu, Y. Xia, Y. S. Hor, D. Qian, A. V. Fedorov, H. Lin, A. Bansil, R. J. Cava, and M. Zahid Hasan, Observation of topological order in a superconducting doped topological insulator, Nat. Phys. 6, 855 (2010).

^[11] M. X. Wang, C. H. Liu, J. P. Xu, F. Yang, L. Miao, M. Y. Yao, C. L. Gao, C. Y. Shen, X. C. Ma, X. Chen, Z. A. Xu, Y. Liu, S. C. Zhang, D. Qian, J. F. Jia, and Q. K. Xue, The coexistence of superconductivity and topological order in the Bi₂Se₃ thin films, Science 336, 52 (2012).

^[12] S. Xu, N. Alidoust, I. Belopolski, A. Richardella, C. Liu, M. Neupane, G. Bian, S. Huang, R. Sankar, C. Fang, B. Dellabetta, W. Dai, Q. Li, J. M. Gilbert, F. Chou, N. Samarth, and Z. M. Hasan, Momentum-space imaging of Cooper pairing in a half-Dirac-gas topological superconductor, Nat. Phys. 10, 943 (2014).

^[13] Y. S. Hor, A. J. Williams, J. G. Checkelsky, P. Roushan, J. Seo, Q. Xu, H. W. Zandbergen, A. Yazdani, N. P. Ong, and R. J. Cava, Superconductivity in CuBiSe, and its Implications for

- Pairing in the Undoped Topological Insulator, Phys. Rev. Lett. **104**, 057001 (2010).
- [14] L. Fu and E. Berg, Odd-Parity Topological Superconductors: Theory and Applications to Cu_xBi₂Se₃, Phys. Rev. Lett. 105, 097001 (2010).
- [15] M. Kriener, K. Segawa, Z. Ren, S. Sasaki, and Y. Ando, Bulk Superconducting Phase with a Full Energy Gap in the Doped Topological Insulator Cu_xBi₂Se₃, Phys. Rev. Lett. 106, 127004 (2011).
- [16] J. Nagamatsu, N. Nakagawa, T. Muranaka, Y. Zenitani, and J. Akimitsu., Superconductivity at 39 K in magnesium diboride, Nature (London) 410, 63 (2001).
- [17] P. Zhang, K. Yaji, T. Hashimoto, Y. Ota, T. Kondo, K. Okazaki, Z. Wang, J. Wen, G. D. Gu, H. Ding, and S. Shin, Observation of topological superconductivity on the surface of an iron-based superconductor, Science 360, 182 (2018).
- [18] S. Tsuda, T. Yokoya, Y. Takano, H. Kito, A. Matsushita, F. Yin, J. Itoh, H. Harima, and S. Shin, Definitive Experimental Evidence for Two-Band Superconductivity in MgB₂, Phys. Rev. Lett. 91, 127001 (2003).
- [19] S. Souma, Y. Machida, T. Sato, T. Takahashi, H. Matsui, S.-C. Wang, H. Ding, A. Kaminski, J. C. Campuzano, S. Sasaki, and K. Kadowaki, The origin of multiple superconducting gaps in MgB₂, Nature (London) 423, 65 (2003).
- [20] S. Tsuda, T. Yokoya, T. Kiss, T. Shimojima, S. Shin, T. Togashi, S. Watanabe, C. Zhang, C. T. Chen, S. Lee, H. Uchiyama, S. Tajima, N. Nakai, and K. Machida, Carbon-substitution dependent multiple superconducting gap of MgB₂: a sub-meV resolution photoemission study, Phys. Rev. B 72, 064527 (2005).
- [21] Y. Sassa, M. Månsson, M. Kobayashi, O. Götberg, V. N. Strocov, T. Schmitt, N. D. Zhigadlo, O. Tjernberg, and B. Batlogg, Probing two- and three-dimensional electrons in MgB₂ with soft x-ray angle-resolved photoemission, Phys. Rev. B 91, 045114 (2015).
- [22] D. Mou, R. Jiang, V. Taufour, S. L. Bud'ko, P. C. Canfield, and A. Kaminski, Momentum dependence of the superconducting gap and in-gap states in MgB₂ multi-band superconductor, Phys. Rev. B 91, 214519 (2015).
- [23] K.-H. Jin, H. Huang, J.-W. Mei, Z. Liu, L.-King Lim, and F. Liu, Topological superconducting phase in high-Tc superconductor MgB₂ with Diracnodal-line fermions, npj Comput. Mater. 5, 57 (2019).

- [24] C. Chiu and A. Schnyder, Classification of reflection symmetry protected topological semimetals and nodal superconductors. Phys. Rev. B **90**, 205136(R) (2014).
- [25] See Supplemental Material at http://link.aps.org/supplemental/ 10.1103/PhysRevB.100.184511 which includes further information on DFT method, sample growth and cleave details, additional ARPES spectra, and comparison to topological superconductivity in FeTe_{1-x}Se_x.
- [26] A. Damascelli, Z. Hussain, and Z. X. Shen, Angle-resolved photoemission studies of the cuprate superconductors, Rev. Mod. Phys. 75, 473 (2003).
- [27] T. Hyart, R Ojajarvi, and T. T. Heikkila, Two topologically distinct Dirac-line semimetal phases and topological phase transitions in rhombohedrally stacked honeycomb lattices, J. Low Temp. Phys. 191, 35 (2018).
- [28] Y.-H. Chan, C.-K. Chiu, M. Y. Chou, and A. P. Schnyder, Ca₃ P₂ and other topological semimetals with line nodes and drumhead surface states, Phys. Rev. B **93**, 205132 (2016).
- [29] S.-Y. Xu, I. Belopolski, N. Alidoust, M. Neupane, G. Bian, C. Zhang, R. Sankar, G. Chang, Z. Yuan, C.-C. Lee, S.-Ming Huang, H. Zheng, J. Ma, D. S. Sanchez, B. K. Wang, A. Bansil, F. Chou, P. P. Shibayev, H. Lin, S. Jia, and M. Zahid Hasan, Discovery of a Weyl fermion semimetal and topological Fermi arcs, Science 349, 613 (2015).
- [30] J. D. Koralek, J. F. Douglas, N. C. Plumb, Z. Sun, A. V. Fedorov, M. M. Murnane, H. C. Kapteyn, S. T. Cundiff, Y. Aiura, K. Oka, H. Eisaki, and D. S. Dessau, Laser Based Angle-Resolved Photoemission, the Sudden Approximation and Quasiparticle-Like Spectra peak in Bi₂Sr₂CaCu₂O_{8+δ}, Phys. Rev. Lett. 96, 017005 (2006).
- [31] T. Shimojima, K. Okazaki, and S. Shin, Low-temperature and high-energy-resolution laser photoemission spectroscopy, J. Phys. Soc. Jpn. 84, 072001 (2015).
- [32] X. X. Xi, MgB thin films, Supercond. Sci. Technol. 22, 043001 (2009).
- [33] D. Wang, L. Kong, P. Fan, H. Chen, S. Zhu, W. Liu, L. Cao, Y. Sun, S. Du, J. Schneeloch, R. Zhong, G. Gu, L. Fu, H. Ding, and H.-J. Gao, Evidence for Majorana bound states in an iron-based superconductor, Science 362, 333 (2018).
- [34] S.-Y. Yang, H. Yang, E. Derunova, S. S. P. Parkin, B. Yan, and M. N. Ali, Symmetry demanded topological nodal-line materials, Adv. Phys. X 3, 1414631 (2018).